Time-dependent driving and topological protection in the fractional Josephson effect

Ahmed Kenawy,[1] Fabian Hassler,[2] and Roman-Pascal Riwar[1]
[1]*Peter Grünberg Institut, Forschungszentrum Jülich, D-52425 Jülich, Germany*
[2]*Institute for Quantum Information, RWTH Aachen University, 52056 Aachen, Germany*

(Received 29 June 2023; revised 6 May 2024; accepted 4 June 2024; published 18 June 2024)

The control of any type of quantum hardware invariably necessitates time-dependent driving. If the basis depends on the control parameter, the presence of a time-dependent control field yields an extra term in the Schrödinger equation that is often neglected. Here, we examine the effect of this term in a flux-controlled Majorana junction. We show that a time-varying flux gives rise to an electromotive force, which is highly nonlinear when truncating to the junction's low-energy degrees of freedom. As a result, it compromises the robustness of the ground-state degeneracy present in the absence of the drive. The resulting flattening of the energy spectrum can be measured by a strong suppression of the dc supercurrent.

DOI: 10.1103/PhysRevB.109.245423

I. INTRODUCTION

Topological insulators and other noninteracting systems can be classified according to their symmetries, using the tenfold way [1–4]. In realistic systems, the topologically protected ground-state degeneracy can be compromised by several processes. But such processes are commonly expected to be exponentially suppressed, such as the overlap of Majorana edge modes [5,6], or similarly the overlap of edge modes in topological insulators [7–9]. The topological protection becomes algebraic in one-dimensional (1D) superconductors [10,11] or when coupled to a dissipative environment [12–14], which, among others, motivates extending the concept of topological phases to non-Hermitian Hamiltonians of open systems [15–27].

An even more basic problem is the interplay between topological protection and classical time-dependent driving. Given a Hamiltonian system that depends on a tunable control parameter x, it is common to include driving parametrically—that is, $H(x) \to H[x(t)]$—which implies that the time-dependent system inherits the symmetries and topological protection from its stationary counterpart. But if the basis of H depends on x, the Schrödinger equation acquires the additional term[1] $-i\dot{x}U^\dagger\partial_x U$ where the unitary $U(x)$ encodes the basis [28]. In the adiabatic limit, this term corresponds to the Berry connection. Importantly, this term is often neglected and hence the fate of the topological protection in the presence of time-dependent driving is still largely unexplored.

In order to address this fundamental question, we study superconducting circuits. Here, the influence and microscopic origin of the term $-i\dot{x}U^\dagger\partial_x U$ have recently been examined for generic superconducting circuits driven by time-dependent flux [29–31], in which case this term represents an electromotive force (emf). To include the aspect of topological protection, we choose to study the basic example of Majorana fermions in p-wave superconductors, which may be realized in various condensed-matter systems [32–40], for example, proximitized semiconducting nanowires [41,42]. The study of the resulting fractional Josephson effect [33,43] has seen a revival on theory side [44–50], specifically the interplay of time-dependent driving and dissipation, along with the role of the overlap between edge modes in transport across the junction. Nonetheless, full understanding of the experimentally observed suppression of the first Shapiro step and of the Landau-Zener probability in the qubit formed by coupling two Majoranas across the weak link [51–59] is still a topic of active research.

In this work, we study the effect of the emf on topological protection in Majorana junctions, where the control parameter is the phase bias ϕ across the junction. Building on previous results valid at weak driving [60], here, we account for the effect of the emf to all (relevant) orders. By eliminating high-energy quasiparticle states, we demonstrate that while the emf term for the full system Hamiltonian is by construction linear in the voltage $V = \dot{\phi}/(2e)$, its effect on the low-energy description is amplified, resulting in a highly nonlinear renormalization of the effective Majorana overlap for the driven junction. Moreover, we show that this effect strongly suppresses the supercurrent, as evidenced by the IV characteristics of the driven junction. This result entails modifications of various predictions regarding time-dependent driving of Majorana junctions (e.g., Refs. [51–59]). In general, we show that an accurate theoretical description of driven (topological) quantum systems needs the careful treatment of the dependence of the basis on the external control parameter.

II. MODEL

We consider a flux-controlled Majorana junction, which consists of two tunnel-coupled topological superconductors. We model the superconductors as one-dimensional Kitaev chains with nearest-neighbor hopping and pairing [5,61]. The two contacts have a phase difference $\phi \equiv \phi_R - \phi_L$ that is generally time dependent (Fig. 1). The central question of

[1]Here and in the following, we set $\hbar = 1$.

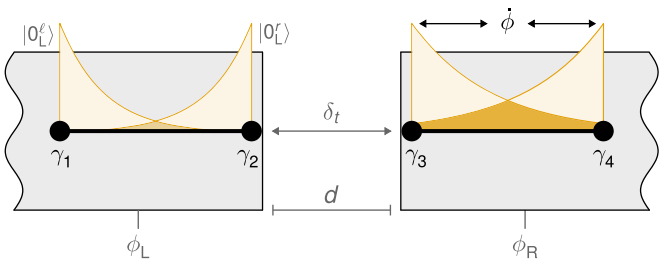

FIG. 1. Two tunnel-coupled topological superconducting wires, represented by the four Majoranas $\{\gamma_1, \gamma_2, \gamma_3, \gamma_4\}$. The wires are placed on top of two superconductors (gray), which interconnect at the far ends to form a loop threaded by a time-dependent magnetic field. The applied field leads to a phase difference $\phi = \phi_R - \phi_L$. The phase drop is included entirely in the right wire. The induced emf (owing to the time-dependent phase) strongly modifies the coupling between Majoranas γ_3 and γ_4, which can be regarded as a strong renormalization of the overlap between the exponential tails of the Majoranas.

this work is how to incorporate the time-dependent phase difference due to the bias voltage in the Hamiltonian description of the system. The most common choice is to attach ϕ to the tunneling across the weak link, which leads to the Hamiltonian

$$H = H_L + H_T(\phi) + H_R. \tag{1}$$

The individual Kitaev chains (of J sites) are described by

$$H_\alpha = -\mu \sum_j^J d_{j,\alpha}^\dagger d_{j,\alpha} - t \sum_j^{J-1} (d_{j+1,\alpha}^\dagger d_{j,\alpha} + \text{H.c.}) + \Delta \sum_j^{J-1} (d_{j+1,\alpha} d_{j,\alpha} + \text{H.c.}), \tag{2}$$

where the chain index $\alpha \in \{L, R\}$, t is the hopping amplitude, the chemical potential is within the topological limit $|\mu| \leqslant 2t$, and the pairing potential Δ is real. The operator $d_{j,\alpha}$ annihilates an electron at site j of chain α. The tunneling Hamiltonian reads

$$H_T(\phi) = -\delta t\, (e^{-i\phi/2} d_{1,R}^\dagger d_{J,L} + e^{i\phi/2} d_{J,L}^\dagger d_{1,R}), \tag{3}$$

which couples the two chains with an amplitude $\delta t \ll t$.

The phase difference ϕ could, however, be attached elsewhere in Hamiltonian or, in the most general case, be distributed along a given spatial profile within H. This profile can be encoded in the basis choice of the Hamiltonian via a unitary transformation $U(\phi)$ [29,30,60]. If ϕ is constant in time, these choices are all gauge choices, that is, as long as Cooper pairs acquire the total phase ϕ when traveling from one contact to the other, it does not matter where they acquire it along the way. But the situation is radically different for $\phi \to \phi(t)$. Here, Hamiltonians with different basis choices provide different dynamics [29,30], as different phase profiles correspond to different choices of the vector potential whose time derivative contributes to the (gauge-invariant) electric field [30]. In particular, the choice in Eq. (1) would only be correct if the induced electric field was completely screened by the Kitaev chains. But most materials expected to host Majorana fermions have a low carrier density with poor screening properties. This statement is in accordance with experimental and theoretical data for both semiconducting nanowires [62,63] and 3D topological insulators [64].

Let us now focus on the asymmetric choice for which the phase ϕ is attached to the right Kitaev chain. This choice is described by $\bar{H} = \bar{H}_L + \bar{H}_T + \bar{H}_R(\phi)$ such that

$$\bar{H} = UHU^\dagger = e^{i\phi G_R} H\, e^{-i\phi G_R}, \tag{4}$$

where $G_R = -\sum_j^J d_{j,R}^\dagger d_{j,R}/2$. With this unitary transformation, the phase attaches to the pairing term in the right chain such that $\Delta \to \Delta e^{\pm i\phi}$ for $\bar{H}_R$. The phase distribution in $\bar{H}$ corresponds to the case where the voltage drop $V \equiv \dot{\phi}/(2e)$ occurs between the right chain and the right superconducting bulk. Importantly, we note that for realistic device geometries, the voltage profile as a function of space is much more sophisticated. This fact has been comprehensively studied in our previous work [60] (see also Appendix A, which summarizes these aspects). Note in particular that the main reason why the voltage drop occurs within the nanowires and not at the weak link is that the weak link is typically much smaller than the separation of the superconducting bulks. Ultimately, these details can, however, be disregarded, and we can replace the detailed voltage profile with a constant voltage. If the device geometry is asymmetric, or the external fields are applied asymmetrically, then the simplified picture deployed above is justified. Moreover, we note that a significant part of the here presented phenomenology survives even in a symmetric setup (as long as the voltage drop occurs within the nanowires and not at the weak link). We will comment on the symmetric case again further below.

Low-energy Hamiltonian

We now derive a low-energy description for $\bar{H}$. First, it is useful to transform back into the basis choice that attaches the phase to the weak link (as in H) to ensure that the low-energy basis is ϕ independent. This transformation is accomplished by U as defined in Eq. (4). Due to $\partial_t U \neq 0$, the Schrödinger equation is now governed by $H + \dot{\phi} G_R$, where the second term represents a voltage-induced change of the chemical potential of the right chain.[2]

The second-quantized operators can be written in the form $A_\alpha = \frac{1}{2} \psi_\alpha^\dagger \mathcal{A}_\alpha \psi_\alpha$, where the chain index $\alpha \in \{L, R\}$, the operator $A_\alpha \in \{H_L, H_R, G_R\}$, and the matrix $\mathcal{A}_\alpha \in \{\mathcal{H}_L, \mathcal{H}_R, \mathcal{G}_R\}$. The matrices $\mathcal{H}_\alpha$ and $\mathcal{G}_R$ are constructed such that their product with the field operators $\psi_\alpha = (d_{1,\alpha}, d_{1,\alpha}^\dagger, \ldots, d_{J,\alpha}, d_{J,\alpha}^\dagger)^T$ returns the many-body operators. Likewise, we can write the tunneling Hamiltonian as $H_T(\phi) = \psi_L^\dagger \mathcal{H}_T(\phi) \psi_R$.

For the uncoupled chain Hamiltonians $\mathcal{H}_\alpha = \Sigma_{v_\alpha} \epsilon_{v_\alpha} |v_\alpha\rangle \langle v_\alpha|$, particle-hole symmetry implies that each eigenstate $|v_\alpha\rangle$ at energy ϵ_{v_α} has a pair $|\tilde{v}_\alpha\rangle$ at energy $-\epsilon_{v_\alpha}$, with the two related by $|v_\alpha\rangle = \tau_x |\tilde{v}_\alpha\rangle$ where the Pauli matrix τ_x acts on the Nambu space. The two Majoranas of each chain

[2]The unitary transformation (4) leads to a 4π-periodic Hamiltonian, compared to the 2π-periodic one in Eq. (1). The change of periodicity does not, however, alter the size of the Hilbert space nor the fermion parity.

are related to the states $|0_\alpha\rangle$ and $|\tilde{0}_\alpha\rangle$. If the left and right Majorana modes do not overlap, these states are degenerate at zero energy, which is why we refer to them as the zero-energy states.

For a low-energy description of the full Hamiltonian, we eliminate all but the subspace comprising the zero-energy states $|0_\alpha\rangle$ and $|\tilde{0}_\alpha\rangle$ of each chain, following a standard Schrieffer-Wolff transformation that includes higher-order corrections [65]. This subspace is described by the projection operators $\mathcal{P}_\alpha = |0_\alpha\rangle\langle 0_\alpha| + |\tilde{0}_\alpha\rangle\langle\tilde{0}_\alpha|$, whereas $\mathcal{Q}_\alpha = 1 - \mathcal{P}_\alpha$ projects onto the high-energy quasiparticle states.

The emf term for the full system $\dot{\phi}G_{\mathrm{R}}$ is manifestly linear in $\dot{\phi}$. A central conclusion of our work is that after the projection, this extra term leads to a low-energy description with parameters depending on $\dot{\phi}$ in a highly nonlinear fashion. Namely, we obtain the Hamiltonian

$$H_{\mathrm{low}} = i\frac{\epsilon_0}{2}\gamma_2\gamma_1 + i\frac{\epsilon_0 + g_{\mathrm{R}}}{2}\gamma_4\gamma_3 + iE_{\mathrm{M}}\cos\left(\frac{\phi}{2}\right)\gamma_2\gamma_3, \quad (5)$$

where, in leading order, the weak link only couples γ_2 and γ_3 (Fig. 1), with the operators γ denoting the second-quantized operators of the Majorana modes of each chain, which satisfy $\{\gamma_\mu, \gamma_\nu\} = 2i\delta_{\mu\nu}$. The energy ϵ_0 represents the previously mentioned ordinary overlap between left and right Majorana modes of each chain and equals $\langle 0_\alpha|\,\mathcal{H}_\alpha\,|0_\alpha\rangle$ (where we drop the chain index because we here assume the two chains to have identical parameters for simplicity). The low-energy projection of the extra term $\dot{\phi}G_{\mathrm{R}}$ appears in the Hamiltonian H_{low} in two places: it modifies the Josephson energy $E_{\mathrm{M}}(\dot{\phi})$ and yields a new overlap term $g_{\mathrm{R}}(\dot{\phi})$.

The former originates from the tunneling matrix $\mathcal{H}_{\mathrm{T}}(\phi)$ and couples the two Majoranas γ_2 and γ_3 across the junction. As for its $\dot{\phi}$ renormalization, it is sufficient to account for emf-induced corrections to the Josephson energy E_{M} perturbatively in the form [60]

$$E_{\mathrm{M}}(\dot{\phi}) = \langle 0_{\mathrm{L}}|\,\mathcal{H}_{\mathrm{T}}(0)\,|0_{\mathrm{R}}\rangle - \langle 0_{\mathrm{L}}|\,\mathcal{H}_{\mathrm{T}}(0)\,\frac{\mathcal{Q}_{\mathrm{R}}}{\mathcal{H}_{\mathrm{R}}}\,\dot{\phi}\mathcal{G}_{\mathrm{R}}\,|0_{\mathrm{R}}\rangle\,, \quad (6)$$

where the first term is the standard fractional Josephson effect. The (first-order in $\dot{\phi}$) correction term is the subject of our previous work [60], where it was shown to be measurable either in the linear current response, or (in an open circuit geometry) as an additional contribution to charge fluctuations.

The new overlap term g_{R}—similar to ϵ_0—couples the left and right Majorana modes of the right chain, but the impact of the emf can be much larger in magnitude. To understand this, we pick up on the above observation, that the emf shifts the chemical potential of the right chain as $\mu \to \mu + \dot{\phi}/2$. For $\dot{\phi}$ constant, and neglecting tunneling for now ($H_{\mathrm{T}} = 0$), the problem becomes completely static, such that it suffices to consider the μ dependence of the overlap term. Assuming $t > \delta\mu > \Delta$ ($\delta\mu = 2t + \mu$), the static overlap can be given as $\epsilon_0 \approx \Delta_{\mathrm{F}}\, e^{-J\Delta_{\mathrm{F}}/\tilde{v}_{\mathrm{F}}}\sin(J\delta\mu/\tilde{v}_{\mathrm{F}})$, see Appendix A, where, $\Delta_{\mathrm{F}} \approx 2\Delta\sqrt{\delta\mu/t}$ is the effective local pairing, and $\tilde{v}_{\mathrm{F}} \approx 2\sqrt{t\delta\mu}$ is the Fermi velocity (here in units of energy, since the discrete chain has no length scale).

Note that the only part of the overlap that does not depend on $\delta\mu$ is the coherence length $\xi_0 = \tilde{v}_{\mathrm{F}}/\Delta_{\mathrm{F}}$. The overlap oscillates strongly as a function of $\delta\mu$, where both the oscillation amplitude ($\sim\Delta_{\mathrm{F}}$) and frequency ($\sim 1/\tilde{v}_{\mathrm{F}}$) themselves depend weakly on $\delta\mu$. The oscillations are due to the chain forming a quantum dot, where the oscillations represent the level spacing. Replacing $\delta\mu \to \delta\mu + \dot{\phi}/2$, we thus find a strong voltage-dependent renormalization of the overlap energy of Majoranas in the same chain. Note that the $\dot{\phi}$-renormalization can complete many oscillations before the applied voltage surpasses $2\Delta_{\mathrm{F}}$ (where driving-induced quasiparticle generation leads to a breakdown of the low-energy picture). Consequently, unlike E_{M}, the renormalization of the overlap cannot be obtained perturbatively. It is interesting to note that this phenomenon can be effectively regarded as strong renormalization of the coherence length, $|\epsilon_0| \sim e^{-J/\xi(\dot{\phi})}$ with

$$1/\xi(\dot{\phi}) = 1/\xi_0 - \ln|\sin(J\dot{\phi}/\tilde{v}_F)|/J, \quad (7)$$

where ξ can largely exceed ξ_0. We therefore interpret the phenomenon as a voltage-induced renormalization of the Majorana wave function overlap, as indicated in Fig. 1.

Importantly, the nonperturbative nature of the above effect remains true even if we include the possibility of partial screening within the nanowires, or if the detailed geometry of the device was such that the voltage drop is highly localized. Both of these cases can be easily accounted for by adding a numerical prefactor <1 in front of $\dot{\phi}$. Crucially, such a reduction would, however, only affect the number of oscillations within a given voltage window, but not the amplitude of the oscillations. We further note that for general device geometries, and more complicated fields, there may be dynamical negative capacitance effects (see Ref. [30]), which can increase the numerical prefactor, even to the extent of rendering it >1.

While the above argument holds only for constant $\dot{\phi}$, we now present a generalization to arbitrary driving by means of a partial resummation of higher-order terms in the Schrieffer-Wolff approximation, (ignoring those that are exponentially suppressed in comparison[3]) to obtain (see Appendix B)

$$g_{\mathrm{R}}(\dot{\phi}) = \langle 0_{\mathrm{R}}|\left(\mathbb{1} + \dot{\phi}\mathcal{G}_{\mathrm{R}}\frac{\mathcal{Q}_{\mathrm{R}}}{\mathcal{H}_{\mathrm{R}} - \epsilon_0}\right)^{-1}\dot{\phi}\mathcal{G}_{\mathrm{R}}\,|0_{\mathrm{R}}\rangle\,. \quad (8)$$

The above formula agrees well with the previously discussed analytic overlap term for constant $\dot{\phi}$. Let us at this point interject that the nonlinear renormalization of the overlap does not require spatial asymmetry: it is present even if the voltage drop across the entire junction occurred symmetrically, e.g., where both the pairing on the left and the right chain each acquired $\phi/2$. In this case, $\dot{\phi} \to \dot{\phi}/2$ in Eq. (8), and there would occur a similar renormalization for the overlap of Majoranas on the left.

[3]Within the same order of $\dot{\phi}$, we can compare two terms such as $\mathcal{P}_{\mathrm{R}}\mathcal{G}_{\mathrm{R}}\mathcal{P}_{\mathrm{R}}\mathcal{G}_{\mathrm{R}}\mathcal{Q}_{\mathrm{R}}\mathcal{G}_{\mathrm{R}}\mathcal{P}_{\mathrm{R}}$ and $\mathcal{P}_{\mathrm{R}}\mathcal{G}_{\mathrm{R}}\mathcal{Q}_{\mathrm{R}}\mathcal{G}_{\mathrm{R}}\mathcal{Q}_{\mathrm{R}}\mathcal{G}_{\mathrm{R}}\mathcal{P}_{\mathrm{R}}$. The former depends on the overlap $\mathcal{P}_{\mathrm{R}}\mathcal{G}_{\mathrm{R}}\mathcal{P}_{\mathrm{R}}$ between the exponentially decaying tails of the left and right Majoranas of the right chain, while the latter avoids this suppression and couples solely via the excited states described by the projector $\mathcal{Q}_{\mathrm{R}}$. The former is therefore much smaller and can be dropped. We follow this pattern to obtain the resummation (8).

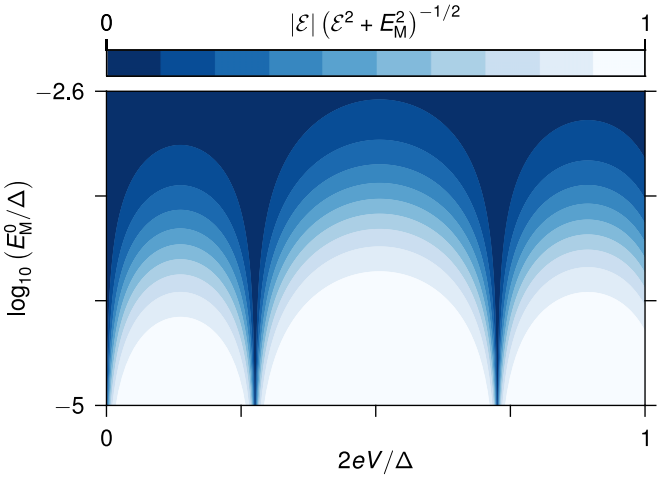

FIG. 2. Impact of the emf on the energy spectrum of Hamiltonian (9) with $p=1$ as a function of the voltage $V=\dot{\phi}/(2e)$ and the unrenormalized Josephson energy $E_{\rm M}^0=E_{\rm M}(\dot{\phi}=0)$. We characterize the spectrum by the ratio $|\mathcal{E}|(\mathcal{E}^2+E_{\rm M}^2)^{-1/2}$ where $\mathcal{E}=g_{\rm R}/2$. The uncoupled Kitaev chains have ground-state degeneracy at zero energy for $V=0$ and $p=1$. The overlap energy $g_{\rm R}$ oscillates as a function of V. Parameters: $J=200$, $\Delta=0.04t$, and $\mu=-1.95t$.

III. RESULTS

To understand the impact of the emf-induced renormalization, we analyze the qubit formed by the coupling of the Majoranas of the left and right chains. We decompose $H_{\rm low}$ into two uncoupled two-level systems for odd and even electron parities. The Hamiltonians of these two subspaces read

$$H_p=-\mathcal{E}\sigma_x+E_{\rm M}\cos\left(\frac{\phi}{2}\right)\sigma_z, \tag{9}$$

where $\mathcal{E}\equiv\delta_{p,0}\,\epsilon_0+g_{\rm R}/2$ with $p=0,1$ for the even and odd parities, respectively. Let us focus on applying a constant voltage ($V=2e\dot{\phi}=$ const.). The driving then provides a constant voltage-dependent renormalization of the energy scales $\mathcal{E}$ and $E_{\rm M}$. The phase ϕ inside the cosine remains the only time-dependent parameter, and a large $g_{\rm R}$ can be regarded as strong gapping of the instantaneous energy spectrum of Hamiltonian H_p. Let us focus on the odd parity ($p=1$) for which the spectrum is gapless in the absence of the drive ($\dot{\phi}=0$). Importantly, the emf-induced gap oscillates as a function of the voltage V. The smaller the Josephson energy $E_{\rm M}^0$ in the absence of the drive (i.e., the worse the quality of the tunnel junction), the more pronounced the oscillations because the spectrum flattens, that is, the overlap energy $g_{\rm R}$ dominates the Josephson energy $E_{\rm M}$. A strong gapping furthermore implies a nearly flat instantaneous eigenspectrum as a function of ϕ, leading to a strongly suppressed supercurrent. To quantify the flatness, we plot the ratio $\mathcal{E}/\sqrt{\mathcal{E}^2+E_{\rm M}^2}$ in Fig. 2 as a function of voltage $V=\dot{\phi}/2e$, where both $g_{\rm R}$ and $E_{\rm M}$ are computed according to Eqs. (6) and (8). Note that the number of oscillations with respect to the voltage can be controlled by the size of the Kitaev chain (see also Appendix A, where we show the overlap oscillations for a larger number of sites per Kitaev chain).

For a realistic description of the time evolution, we include a generic dissipative process. We consider a circuit where the shunt capacitance is very large, such that the phase difference remains to a good approximation classically well defined. If we further assume a very small shunt resistance, applying a current bias exceeding the critical current of the junction effectively translates to a voltage drop applied directly across the junction, such that the above renormalization effect comes into play. In this regime, the dominant dissipation comes from transitions within the internal (Majorana) degrees of freedom. Such processes are captured by the Lindblad master equation

$$\dot{\rho}=-i[H_p,\rho]+\Gamma\,D[L]\rho, \tag{10}$$

where the superoperator $D[L]\rho\equiv L\rho L^\dagger-(1/2)\{L^\dagger L,\rho\}$ represents the relaxation processes and, for simplicity, we only consider parity-conserving processes.[4] It is convenient to work in the instantaneous eigenbasis of Hamiltonian (9), defined by the unitary transformation

$$R=\frac{1}{\sqrt{2}}\begin{pmatrix}\beta_- & \beta_+\\ \mathrm{sgn}(\mathcal{E})\,\beta_+ & -\mathrm{sgn}(\mathcal{E})\,\beta_-\end{pmatrix}, \tag{11}$$

where $\beta_\pm=[1\pm\lambda^{-1}E_{\rm M}\cos(\phi/2)]^{1/2}$ and the absolute value of the eigenvalue of H_p is $\lambda=[\mathcal{E}^2+E_{\rm M}^2\cos^2(\phi/2)]^{1/2}$. In this eigenbasis, the time evolution becomes governed by the Hamiltonian $R^\dagger H_pR-iR^\dagger\dot{R}=-\lambda\,\sigma_z+Y\sigma_y$ with

$$Y\equiv-\dot{\phi}\,\frac{|\mathcal{E}|E_{\rm M}}{4\lambda^2}\,\sin\left(\frac{\phi}{2}\right). \tag{12}$$

For the dissipative term, we consider a single jump operator that relaxes the two-level system to its instantaneous ground state with a rate Γ (i.e., $L=\sigma_-$). This process is consistent with the assumption that the bath is at zero temperature, and its correlation time is much shorter than $(1/\mathcal{E})$ and $(1/E_{\rm M})$. Defining the column vector $|\tilde{\rho}\rangle\rangle=(\tilde{\rho}_{00},\tilde{\rho}_{01},\tilde{\rho}_{10},\tilde{\rho}_{11})^{\rm T}$, with $\tilde{\rho}$ being the density matrix in the instantaneous eigenbasis, leads to the time-evolution equation $|\dot{\tilde{\rho}}\rangle\rangle=\mathcal{L}\,|\tilde{\rho}\rangle\rangle$ with the Liouvillian

$$\mathcal{L}(t)=\begin{pmatrix}0 & -Y & -Y & \Gamma\\ Y & 2i\lambda-\frac{\Gamma}{2} & 0 & -Y\\ Y & 0 & -2i\lambda-\frac{\Gamma}{2} & -Y\\ 0 & Y & Y & -\Gamma\end{pmatrix}. \tag{13}$$

Here, we are interested in how the emf-induced renormalization of the parameters modifies the IV characteristics of the driven junction. The expected value of the current is defined as $\mathrm{Tr}(\tilde{\rho}\tilde{I})$, where the current operator $\tilde{I}$ in the instantaneous eigenbasis equals $R^\dagger IR$ with

$$I=eE_{\rm M}\,\sin\left(\frac{\phi}{2}\right)\sigma_z. \tag{14}$$

[4] At least for topologically trivial junctions, experimental evidence suggests that parity flips can be made rare [66]. The parity-conserving relaxation process we introduce here could for instance arise from flux noise, and is sufficient for qualitatively realistic predictions since the Hamiltonian H_p depends weakly on p.

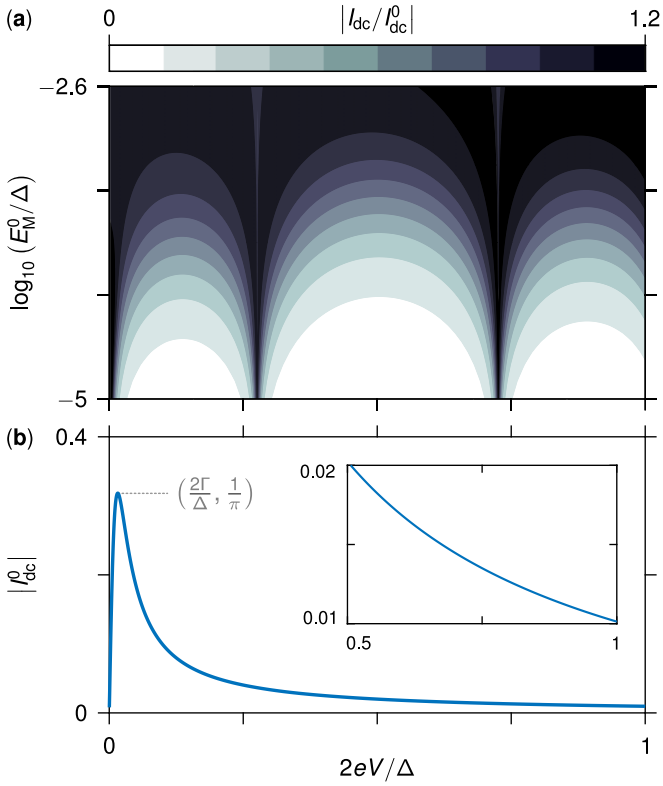

FIG. 3. Steady-state dc current across the junction. (a) The dc current I_{dc} as a function of the applied voltage $V = \dot{\phi}/(2e)$. We choose to normalize it with respect to I^0_{dc}, the current without $\dot{\phi}$ renormalization. The ratio I_{dc}/I^0_{dc} is strongly suppressed, especially at weaker tunneling between the two Kitaev chains. The oscillations with respect to the voltage reflect the behavior of the energy spectrum in Fig. 2. (b) The dc current I^0_{dc} is normalized by the critical current $e|E^0_M|$. The chain parameters are the same as Fig. 2. The relaxation rate $\Gamma = \Delta/(40\pi)$ so that, in the range of voltages considered, the dynamics are not dominated by relaxation.

In a transient state (when the system did not have time to relax) the current does not need to have any particular periodicity in time. In the steady state, however, the current defaults to 2π periodicity because the system is given sufficient time to mix between the two available states. Here, we focus on the dc current I_{dc}, compared to the current I^0_{dc} without renormalization [i.e., substituting with $E^0_M \equiv E_M(\dot{\phi} = 0)$ and $g_R(\dot{\phi} = 0) = 0$ in H_p]. The unrenormalized parameters correspond to assigning the entire time-dependent phase difference to the weak link as in Eq. (1)—the default assumption previous to our work.

Let us again discuss the odd parity $p = 1$. Without renormalizing the parameters, the spectrum of the driven junction is still gapless. In this case, the steady-state dc current has the analytical solution (see Appendix C)

$$I^0_{dc} = -\frac{1}{\pi}\frac{4\Gamma\dot{\phi}}{4\Gamma^2 + \dot{\phi}^2}, \tag{15}$$

which is in units of the critical current $e|E^0_M|$. The dependence of the current I^0_{dc} on the voltage $V = \dot{\phi}/(2e)$ is depicted in Fig. 3(b).

Using the renormalized parameters, on the other hand, reveals that the time-dependent phase $\dot{\phi}$ results in a much richer physics for the driven system, as captured by Fig. 3(a). The dc current in the steady state exhibits the same structure as the spectrum in Fig. 2, reflecting the fact that the flattening of the instantaneous spectrum indeed suppresses the current across the junction. Moreover, the smaller the Josephson energy E^0_M (i.e., the worse the quality of the tunnel junction), the stronger the effect of renormalizing the parameters. This behavior demonstrates one of our main results: the initially linear emf correction term $-i\dot{\phi}U^\dagger\partial_\phi U$ can yield a strongly nonlinear effect on the system dynamics when projected to the low-energy subspace.

IV. CONCLUSION

We study the interplay between topological protection and a classical time-dependent driving through the representative example of Majorana junctions. By deriving a low-energy theory, we show that the induced electromotive force (emf) modifies the Josephson energy and enhances the effective overlap between the left and right Majorana modes of the nanowires. The renormalization of these two energy scales manifests as a strong suppression in the steady-state dc current across the junction. Future works include analyzing the current noise, as well as the impact of ac voltage driving, where the strong $\dot{\phi}$ oscillations of the overlap are expected to amplify transitions between low-energy states for long Kitaev chains. Our work illustrates the importance of a proper microscopic description of the coupling between a given quantum system and the control parameter. Finally, we note that the central ingredients for the physics discussed in this paper (time-dependent control in the presence of a time-dependent basis and the exponential suppression of topological edge-state overlap) transcend the narrow context of Majorana systems. It remains therefore an interesting topic for future research to extend the analysis presented in this paper to the protection of other topological systems.

ACKNOWLEDGMENTS

This work is supported by the Bavarian Ministry of Economic Affairs, Regional Development and Energy within Bavaria's High-Tech Agenda Project "Bausteine für das Quantencomputing auf Basis topologischer Materialien mit experimentellen und theoretischen Ansätze" (Grant No. 07 02/686 58/1/21 1/22 2/23). R.-P. Riwar acknowledges funding from the German Federal Ministry of Education and Research within the program "Photonic Research Germany" (Contract No. 13N14891).

APPENDIX A: MAJORANA BOUND STATES AND PHASE DROP

In this section, we first provide an analytic treatment of the Majorana overlap term as a function of the chemical potential, as discussed in the main text. We then argue with the example of coplanar capacitor geometry, why it is justified to effectively treat the voltage drop due to the drive ($\sim\dot{\phi}$) as a shift in the chemical of the Kitaev chains (see also Ref. [60]).

1. Energy gap of Majoranas within the same chain for constant voltage

Consider the Kitaev chain Hamiltonian of the form of Eq. (2) in the main text. For our purpose here, it is convenient to translate the discrete model in the main text to a continuous model, where the dimensionless wave vector q from the discrete model (e.g., without pairing, electrons move in plain waves $\sim e^{ijq}$) is translated to the wave vector $k = q/\Delta x$, with Δx being a length scale separating the discrete sites (where plain waves are $\sim e^{ikx}$ with $x/\Delta x = j$).

In addition, assuming $t > \delta\mu > \Delta$ ($\mu = -2t + \delta\mu$), we consider a regime where the bare electron and hole dispersion relation can be linearized, such that it is justified to separate the k space into left and right movers, where $k \approx \pm k_F + \delta k$, and $k_F \Delta x \approx \sqrt{\delta\mu/t}$. In this regime, the originally nonlocal pairing Δ gets rescaled to a local pairing $\Delta_F = 2\Delta \sin(q_F) \approx 2\Delta\sqrt{\delta\mu/t}$. Note that due to the Fermi wave vector appearing in Δ_F, the local pairing aquires a sign depending on whether it couples left or right movers. The resulting Schrödinger equation can be written as

$$\tfrac{1}{2} h|\psi(x)\rangle = E|\psi(x)\rangle \tag{A1}$$

with the Bogoliubov-de Gennes Hamiltonian

$$h = -(i v_F \partial_x \sigma_z + \delta\mu)\tau_z - \Delta_F \sigma_z \tau_y, \tag{A2}$$

where the Pauli matrix σ_z represents the left- and right-mover basis, and $\tau_{z,y}$ refer to the Nambu space. The Fermi velocity is simply given as $v_F/\Delta x = 2\sqrt{t\delta\mu}$. The prefactor $1/2$ on the left-hand side is due to fermion doubling (in accordance with the definition $A_\alpha = \frac{1}{2}\psi_\alpha^\dagger \mathcal{A}_\alpha \psi_\alpha$ in the main text).

Hamiltonian (A2) conserves left and right movers ($[\sigma_z, h] = 0$). Therefore, at least in the bulk, it can be diagonalized separately for left and right movers, such that we may take the full four-component wave function $|\psi(x)\rangle$ and select out either left movers ($\sigma_z = -1$) or right movers ($\sigma_z = +1$)

$$[|\psi(x)\rangle]_\pm = \begin{pmatrix} u_x^\pm \\ v_x^\pm \end{pmatrix}. \tag{A3}$$

The remaining two-component vector represents the Nambu space. The hard walls at the edges ($x = 0, L$) on the other hand couple left and right movers, with the hard-wall boundary condition

$$\begin{pmatrix} u_{0,L}^+ \\ v_{0,L}^+ \end{pmatrix} = -\begin{pmatrix} u_{0,L}^- \\ v_{0,L}^- \end{pmatrix}. \tag{A4}$$

The minus sign will turn out to be irrelevant for the computation of eigenenergies, but provides the correct sin-wave behavior for the particle in a box solutions, simply due to $e^{ikx} - e^{-ikx} \sim \sin(kx)$. Now, when propagating the wave function from $x = 0$ to $x = L$, we find that the boundary conditions give rise to the eigenvalue problem

$$\begin{pmatrix} u_0^+ \\ v_0^+ \end{pmatrix} = e^{2i\frac{L}{v_F}\delta\mu} Q(E) \begin{pmatrix} u_0^+ \\ v_0^+ \end{pmatrix}, \tag{A5}$$

where we defined the matrix

$$Q(E) = e^{i\frac{L}{v_F}(\tau_z 2E - \Delta_F \tau_z \tau_y)} e^{i\frac{L}{v_F}(\tau_z 2E + \Delta_F \tau_z \tau_y)}. \tag{A6}$$

The first phase prefactor $e^{2ik_F L}$ comes from including the fast oscillating phase in the propagation due to k_F. As can be seen, all it does is provide a meaningful reference point for $\delta\mu$. For the Majorana bound states, we need to find the value of $2E < \Delta_F$, such that $e^{2i\frac{L}{v_F}\delta\mu} Q(E)$ has eigenvalue 1.

Defining $\epsilon = 2LE/v_F$, $\delta = L\Delta_F/v_F$, and $\xi = \sqrt{\delta^2 - \epsilon^2}$ we find for the matrix Q

$$Q(E) = \frac{\delta^2 - \epsilon^2 \cosh(2\xi)}{\xi^2} + i\frac{\epsilon \sinh(2\xi)}{\xi}\tau_z - \frac{\epsilon\delta[\cosh(2\xi) - 1]}{\xi^2}\tau_y. \tag{A7}$$

Its eigenvalues are therefore

$$\frac{\delta^2 - \epsilon^2 \cosh(2\xi)}{\xi^2} \pm \sqrt{\left(\frac{\delta^2 - \epsilon^2 \cosh(2\xi)}{\xi^2}\right)^2 - 1}. \tag{A8}$$

Note that for the eigenvalues of $Q(E)$ to cancel the phase $e^{2i\frac{L}{v_F}\delta\mu}$, they need to be complex numbers with absolute value 1. For $|\epsilon| < \delta$, this can only be the case if

$$\frac{\delta^2 - \epsilon^2 \cosh(2\sqrt{\delta^2 - \epsilon^2})}{\delta^2 - \epsilon^2} < 1, \tag{A9}$$

such that the above square root term is imaginary. In fact, assuming $\delta > 1$ (weak overlap between Majorana bound states), this can only occur for $|\epsilon| \ll \delta$, such that we can expand the above expression for up to first order in ϵ^2. We thus obtain the condition

$$\cos\left(2\frac{L}{v_F}\delta\mu\right) = 1 - \frac{1}{2}\frac{\epsilon^2}{\delta^2} e^{2\delta}, \tag{A10}$$

which is solved as

$$\epsilon = \pm 2\delta e^{-\delta} \sin\left(\frac{L}{v_F}\delta\mu\right). \tag{A11}$$

Inserting back in the definitions for ϵ and δ, this results in

$$E = \pm\Delta_F e^{-\frac{L}{v_F}\Delta_F} \sin\left(\frac{L}{v_F}\delta\mu\right). \tag{A12}$$

Finally, we can return to the discrete model, where we simply replace $L/\Delta x = J$ and define $\widetilde{v}_F = v_F/\Delta x$ which has the units of energy. In the main text, this energy solution is defined as ϵ_0.

As also stated in the main text, the above formula can be extended to the time-dependent problem by $\delta\mu \to \delta\mu + \dot{\phi}/2$. In Fig. 4, we compare the above analytic result with the exact numeric calculation of the discrete chain model, Eq. (2) in the main text, and the resulting overlap from the renormalization calculation presented in the following Appendix B, as a function of $\dot{\phi}$. All three results agree well.

Finally, as can be seen in Eq. (A12), the oscillations of the overlap energy as a function of voltage scale with the size of the Kitaev chain. This fact is demonstrated in Fig. 5, where we double the number of lattice points in the Kitaev chain with respect to Fig. 2 in the main text.

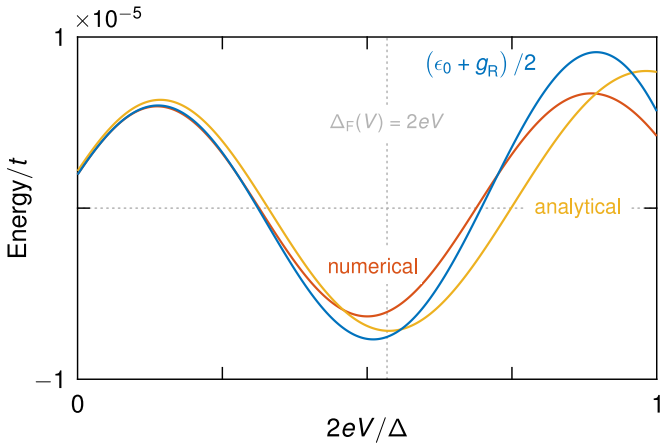

FIG. 4. Ground-state energy of a Kitaev chain in the presence of an induced voltage $V = \dot{\phi}/(2e)$. As derived in Eq. (B32), the low-energy Hamiltonian for the right chain is $(\epsilon_0 + g_R)/2\,\sigma_z$ where σ_z is the Pauli matrix. Here, we compare three methods to calculate the ground-state energy, the resummation (blue) of the overlap term given in Eq. (8) in the main text, the numerical (red) diagonalization of the matrix $(\mathcal{H}_R + \mathcal{G}_R)$, and the analytical (orange) solution in Eq. (A12). The vertical dotted line corresponds to point at which the local pairing Δ_F equals the voltage $2\,eV$.

2. Why the phase must be attached to the nanowire-superconductor interface

In the Hamiltonian of the main text, Eq. (4), we consider attaching the time-dependent phase at the nanowire-superconducting interface, equivalent to having a dominant (constant) voltage within the wires (see also Appendix A 1 above). As worked out in detail in our previous work, Ref. [60], this coupling provides the qualitatively correct description of the flux drive for realistic geometries for the Majorana device. We here reiterate the reasoning of Ref. [60] for completeness. The argumentation follows four main steps, as also depicted in Fig. 6.

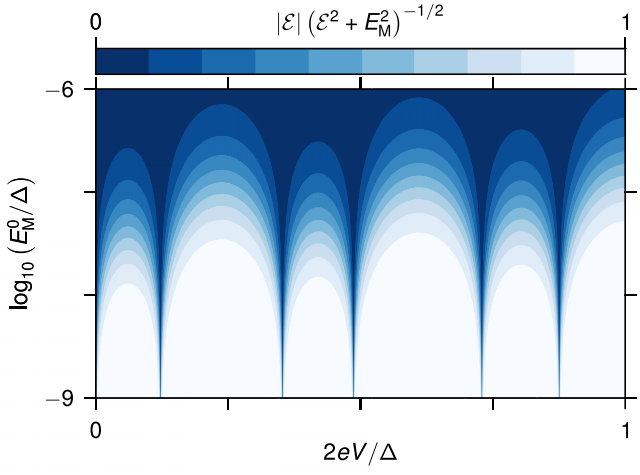

FIG. 5. The ratio $|\mathcal{E}|(\mathcal{E}^2 + E_M^2)^{-1/2}$ where $\mathcal{E} = g_R/2$ plotted as a function of the applied voltage $V = \dot{\phi}/(2e)$. All parameters are the same as in Fig. 2 in the main text, except for the number of lattice sites, which is here $J = 400$ instead of $J = 200$. As a consequence, this doubles the frequency of oscillations as a function of V.

First, we notice that for typical nanowire heterostructure, not all of the wire is proximitized. That is, at the weak link part of the wire is typically exposed, see Fig. 6(a). Next, as already justified in the main text, we assume that electric fields are only expelled from the superconducting bulk, whereas the nanowires are poor screeners. Consequently, the electric field (and thus, the vector potential in the irrotational gauge [29,30]) simply follows the standard solution of a coplanar capacitor, see again Fig. 6(a).

As a result, the voltage drop occurs mostly in between the two superconducting plates (where the field lines are most concentrated). Crucially, since the separation of the superconducting bulks is typically much larger than the actual size of the weak link (where tunneling occurs), the voltage drops in large majority in the nonproximitized region of the bulk nanowire—and not at the weak link itself, see Figs. 6(b) and 6(c). We further note that due to the finite nanowire thickness, the phase profile in the coplanar geometry enters as an algebraically decaying tail into the proximitized part of the wires, whose integral is not necessarily vanishing very quickly.

Importantly, in the Hamiltonian in Eq. (4), both left and right Kitaev chains are fully proximitized (all sites have a finite p-wave pairing), such that it may seem as if Eq. (4) cannot incorporate the finite voltage profile in the unproximitized part. Here we show that even this part can be effectively included as an overlap integral within a fully proximitized version of the wire [see Fig. 6(d)]. This fact was already used in Ref. [60], but was not explicitly demonstrated. Deploying again the low-energy left- and right-mover Hamiltonian for a single wire in Eq. (A2), we can account for the phase profile in that wire by adding the corresponding voltage $\dot{\phi}_\alpha(x)$. We can perform this step for the left or the right chain $\alpha = \mathrm{L,R}$ separately. As pointed out already in the main text, if, e.g., the device geometry is asymmetric, the voltage mostly couples only to one chain only, see Fig. 6(c). For both chains, we obtain a Hamiltonian of the form

$$h = -(iv_F\,\partial_x\sigma_z + \delta\mu + \dot{\phi}(x)/2)\tau_z - \Delta_F(x)\sigma_z\tau_y. \qquad \text{(A13)}$$

Note that here, we include explicitly the spatial dependence of the pairing Δ_F to distinguish between the proximitized ($\Delta_F \neq 0$) and the nonproximitized ($\Delta_F = 0$) part of the wire. For concreteness, let us explicitly work through the example of the right wire ($\alpha = \mathrm{R}$). We here choose the coordinate x of a single wire such that the unproximitized part runs from $0 < x < l$, whereas the proximitized part runs from $l < x < L$. For $l < x < L$, the corresponding part of the phase profile is obviously accounted for by an overlap integral with the Majorana wave functions. The computation of the resulting energy levels works similarly to the solution presented in Eqs. (A5) and (A6), except that now for the calculation of the propagator $Q(E)$, we have in general to do path ordering along x space since the Hamiltonian h at different positions does no longer commute.

In order to include the part from $x = 0$ to $x = l$, we can exploit the fact that with $\Delta_F = 0$, the Hamiltonian again commutes for different x. Consequently, this final piece is conveniently included by substituting

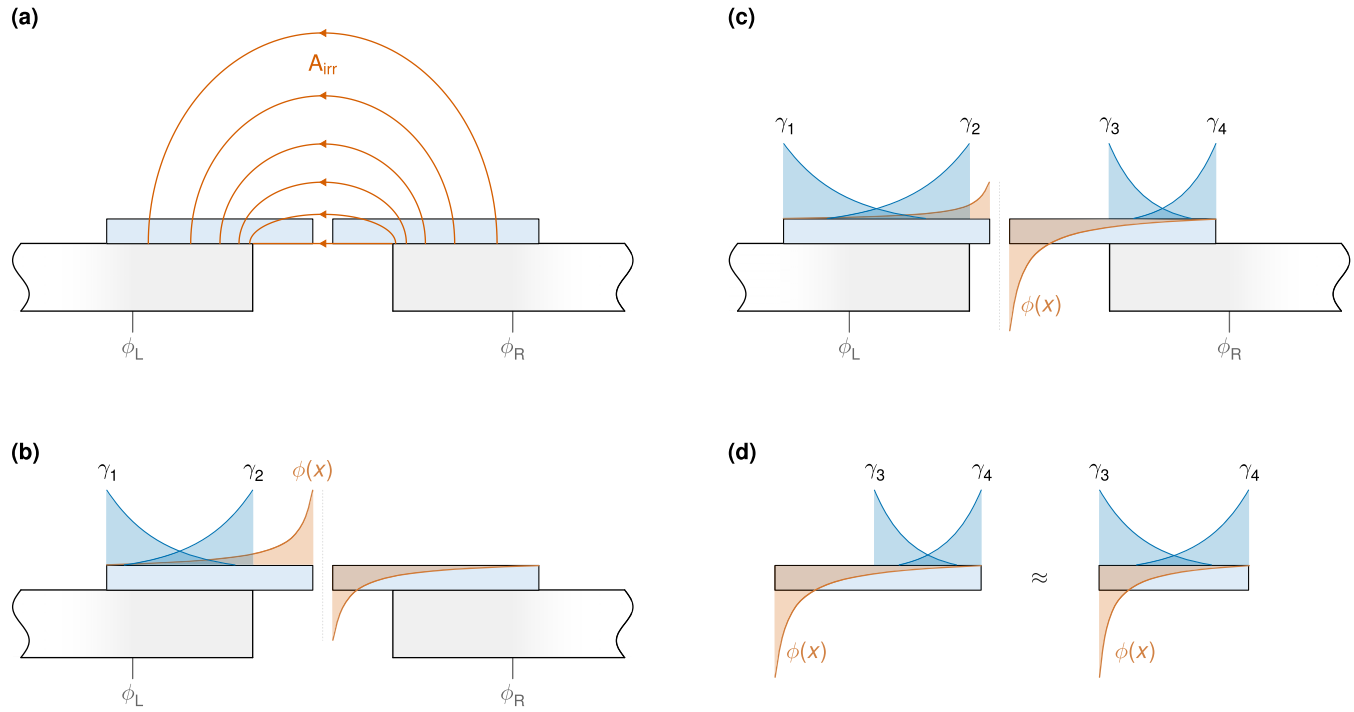

FIG. 6. Step by step derivation of the model with dominant phase drop in the nanowires, as shown in Fig. 1 (see also Ref. [60]). (a) We assume that the electric field is weakly screened within the nanowires, such that the induced electric field (and thus, the vector potential in the irrotational gauge [29,30]) penetrates them. Due to the suspended bridge geometry (and the weak link being much smaller than the distance between bulk superconductors), the phase drop occurs mostly within the nanowires, with the phase profile being (b) symmetric or (c) asymmetric, depending on the device geometry. (d) It can be demonstrated that the phase drop can be effectively included as an overlap integral with the Majorana wave functions, in spite of the overlap not being exact.

$\delta\mu \to \delta\mu + \int_0^l dx\dot{\phi}(x)/2$ in Eq. (A5). If the Majorana bound state wave functions are localized on a length larger than l, the full problem is very accurately described by replacing the complicated problem including the exposed part of the wire with an analog system with fully proximitized wires (right up to the weak link) and shifting the voltage profile of the original problem into the proximitized part, as shown schematically in Fig. 6(d). Finally, we can replace the complicated realistic voltage profile simply with a constant voltage contribution within the wire. For a localized voltage this is exact up to a numerical prefactor, which accounts for the details of the overlap between voltage profile and Majorana wave functions. For very strongly localized voltage profile, this prefactor may be small. We stress though that realistically, the voltage profile has an algebraic tail, which does not vanish quickly. Second, for more general geometries and applied fields, which touch the superconductor, there may be dynamical negative capacitance effects (first described in Ref. [30]), which can massively increase the numerical prefactor and easily compensate for a strong localization of the voltage profile.

APPENDIX B: LOW-ENERGY DESCRIPTION FOR THE DRIVEN JUNCTION

In the basis that attaches the entire phase difference (between the two superconductors in Fig. 1) to the weak link, the time-dependent Schrödinger equation is governed by $H + \dot{\phi}G_R$, where H is given in Eqs. (1)–(3), whereas G_R is defined below Eq. (4) in the main text.

In the Bogoliubov-de Gennes (BdG) form, the Hamiltonian can be written as

$$\begin{aligned} H &= \frac{1}{2}\psi^\dagger \mathcal{H}\psi \\ &= \frac{1}{2}(\psi_L^\dagger \quad \psi_R^\dagger)\begin{pmatrix} \mathcal{H}_L & \mathcal{H}_T(\phi) \\ \mathcal{H}_T^\dagger(\phi) & \mathcal{H}_R \end{pmatrix}\begin{pmatrix} \psi_L \\ \psi_R \end{pmatrix}, \end{aligned} \tag{B1}$$

where $\psi_\alpha = (d_{1,\alpha}, d_{1,\alpha}^\dagger, \ldots, d_{J,\alpha}, d_{J,\alpha}^\dagger)^T$. In terms of its eigenstates, the uncoupled chain Hamiltonians can be decomposed as

$$\mathcal{H}_\alpha = \sum_{v_\alpha} \epsilon_v |v_\alpha\rangle\langle v_\alpha| - \epsilon_v |\tilde{v}_\alpha\rangle\langle\tilde{v}_\alpha| . \tag{B2}$$

Each eigenstate $|v_\alpha\rangle$ at energy ϵ_{v_α} has a pair $|\tilde{v}_\alpha\rangle$ at energy $-\epsilon_{v_\alpha}$, with the two related by $|v_\alpha\rangle = \tau_x|\tilde{v}_\alpha\rangle$ where the Pauli matrix τ_x acts on the particle and hole blocks. The two Majoranas of each chain are related to the states $|0_\alpha\rangle$ and $|\tilde{0}_\alpha\rangle$, which are degenerate at zero energy if the left and right Majorana modes do not overlap. The tunneling matrix can be written as

$$\mathcal{H}_T^{j,j'}(\phi) = \delta_{j,J}\,\delta_{j',1}\begin{pmatrix} -\delta_t\, e^{-i\phi/2} & 0 \\ 0 & \delta_t\, e^{i\phi/2} \end{pmatrix}. \tag{B3}$$

Finally, the operator G_{R} reads

$$G_{\mathrm{R}} = \frac{1}{2}\psi^{\dagger}\begin{pmatrix} 0 & 0 \\ 0 & \mathcal{G}_{\mathrm{R}} \end{pmatrix}\psi, \tag{B4}$$

where $\mathcal{G}_{\mathrm{R}} = -\tau_z/2$.

Our goal is to obtain a Hamiltonian that describes the low-energy subspace defined by the projector

$$\mathcal{P} = \begin{pmatrix} \mathcal{P}_{\mathrm{L}} & 0 \\ 0 & \mathcal{P}_{\mathrm{R}} \end{pmatrix} = \sum_{v=0,\tilde{0}} \begin{pmatrix} |v_{\mathrm{L}}\rangle\langle v_{\mathrm{L}}| & 0 \\ 0 & |v_{\mathrm{R}}\rangle\langle v_{\mathrm{R}}| \end{pmatrix}. \tag{B5}$$

We derive the low-energy Hamiltonian by decoupling the subspace comprising the four states $\{|0_{\mathrm{L}}\rangle, |\tilde{0}_{\mathrm{L}}\rangle, |0_{\mathrm{R}}\rangle, |\tilde{0}_{\mathrm{R}}\rangle\}$ from the high-energy states defined by $\mathcal{Q} = 1 - \mathcal{P}$ via a perturbative expansion in the tunneling amplitude δt and $\dot{\phi}$. We focus on processes that are first order in δ_t but account for higher orders in $\dot{\phi}$. The general form of the low-energy Hamiltonian can be written as

$$H_{\mathrm{low}} = H^{(0)}_{\mathrm{low}} + H^{(1)}_{\mathrm{low}} + H^{(2)}_{\mathrm{low}} + \ldots, \tag{B6}$$

where the order of H^{n}_{low} denotes the sum of the orders of both δ_t and $\dot{\phi}$. The form of the Schrieffer-Wolff transformation can be found in Ref. [65]. For the zeroth order in δ_t and $\dot{\phi}$, we have

$$\begin{aligned} H^{(0)}_{\mathrm{low}} &= \frac{1}{2}\sum_{\alpha}\psi^{\dagger}_{\alpha}(\mathcal{P}_{\alpha}\mathcal{H}_{\alpha}\mathcal{P}_{\alpha})\psi_{\alpha} \\ &= \frac{1}{2}\sum_{\alpha}\psi^{\dagger}_{\alpha}\left(\sum_{x_\alpha,y_\alpha} h^{\alpha}_{xy}\,|x_{\alpha}\rangle\langle y_{\alpha}|\right)\psi_{\alpha}, \end{aligned} \tag{B7}$$

where $\{x, y\} \in \{0, \tilde{0}\}$ and $h^{\alpha}_{xy} = \langle x_{\alpha}|\,\mathcal{H}_{\alpha}\,|y_{\alpha}\rangle$. The matrix element reads

$$\langle 0_{\alpha}|\,\mathcal{H}_{\alpha}\,|0_{\alpha}\rangle = -\langle\tilde{0}_{\alpha}|\,\mathcal{H}_{\alpha}\,|\tilde{0}_{\alpha}\rangle = \epsilon_0, \tag{B8}$$

where the subscript α is dropped for the energy ϵ_0 because we assume that the two chains have the same parameters—namely, t, μ, and Δ. The zeroth-order term then simplifies to

$$\begin{aligned} H^{(0)}_{\mathrm{low}} &= \frac{\epsilon_0}{2}\sum_{\alpha}\psi^{\dagger}_{\alpha}(|0_{\alpha}\rangle\langle 0_{\alpha}| - |\tilde{0}_{\alpha}\rangle\langle\tilde{0}_{\alpha}|)\psi_{\alpha} \\ &= \frac{\epsilon_0}{2}\sum_{\alpha}(c^{\dagger}_{\alpha}c_{\alpha} - c_{\alpha}c^{\dagger}_{\alpha}) \\ &= \frac{\epsilon_0}{2}\sum_{\alpha}(2c^{\dagger}_{\alpha}c_{\alpha} - 1) \\ &= i\frac{\epsilon_0}{2}\gamma_4\gamma_3 + i\frac{\epsilon_0}{2}\gamma_2\gamma_1, \end{aligned} \tag{B9}$$

where the Majorana operators are defined via

$$c_{\mathrm{L}} = \frac{\gamma_2 + i\gamma_1}{2}, \tag{B10}$$

and

$$c_{\mathrm{R}} = \frac{\gamma_4 + i\gamma_3}{2}. \tag{B11}$$

Next, we focus on terms that are zeroth order in δ_t but nonzero in $\dot{\phi}$. In analogy to Eq. (B9), for the right chain, we obtain the overlap energies

$$\frac{i}{2}\left(g^{(1)}_{\mathrm{R}} + g^{(2)}_{\mathrm{R}} + g^{(3)}_{\mathrm{R}} + \ldots\right)\gamma_4\gamma_3, \tag{B12}$$

where the first-order term reads

$$g^{(1)}_{\mathrm{R}} = \langle 0_{\mathrm{R}}|\,\bar{\mathcal{G}}_{\mathrm{R}}\,|0_{\mathrm{R}}\rangle, \tag{B13}$$

with $\bar{\mathcal{G}}_{\mathrm{R}} \equiv \dot{\phi}\mathcal{G}_{\mathrm{R}}$. Similarly, the higher-order contributions read

$$g^{(2)}_{\mathrm{R}} = -\langle 0_{\mathrm{R}}|\bar{\mathcal{G}}_{\mathrm{R}}\frac{\mathcal{Q}_{\mathrm{R}}}{\mathcal{H}_{\mathrm{R}} - \epsilon_0}\bar{\mathcal{G}}_{\mathrm{R}}|0_{\mathrm{R}}\rangle, \tag{B14}$$

and

$$\begin{aligned} g^{(3)}_{\mathrm{R}} = {} & \langle 0_{\mathrm{R}}|\,\bar{\mathcal{G}}_{\mathrm{R}}\frac{\mathcal{Q}_{\mathrm{R}}}{\mathcal{H}_{\mathrm{R}} - \epsilon_0}\bar{\mathcal{G}}_{\mathrm{R}}\frac{\mathcal{Q}_{\mathrm{R}}}{\mathcal{H}_{\mathrm{R}} - \epsilon_0}\bar{\mathcal{G}}_{\mathrm{R}}\,|0_{\mathrm{R}}\rangle \\ & - \langle 0_{\mathrm{R}}|\,\bar{\mathcal{G}}_{\mathrm{R}}\,|0_{\mathrm{R}}\rangle\langle 0_{\mathrm{R}}|\,\bar{\mathcal{G}}_{\mathrm{R}}\frac{\mathcal{Q}_{\mathrm{R}}}{\mathcal{H}_{\mathrm{R}} - \epsilon_0}\frac{\mathcal{Q}_{\mathrm{R}}}{\mathcal{H}_{\mathrm{R}} - \epsilon_0}\bar{\mathcal{G}}_{\mathrm{R}}\,|0_{\mathrm{R}}\rangle. \end{aligned} \tag{B15}$$

Importantly, the second term in $g^{(3)}_{\mathrm{R}}$ is exponentially suppressed compared to the first because it depends on the overlap between the exponentially decaying tails of the left and right Majorana modes through the matrix element $\langle 0_{\mathrm{R}}|\,\bar{\mathcal{G}}_{\mathrm{R}}\,|0_{\mathrm{R}}\rangle$. Conversely, the first term avoids this suppression by coupling exclusively via the excited states, denoted by the projector $\mathcal{Q}_{\mathrm{R}}$. The third-order term then reduces to

$$g^{(3)}_{\mathrm{R}} \approx \langle 0_{\mathrm{R}}|\,\bar{\mathcal{G}}_{\mathrm{R}}\frac{\mathcal{Q}_{\mathrm{R}}}{\mathcal{H}_{\mathrm{R}} - \epsilon_0}\bar{\mathcal{G}}_{\mathrm{R}}\frac{\mathcal{Q}_{\mathrm{R}}}{\mathcal{H}_{\mathrm{R}} - \epsilon_0}\bar{\mathcal{G}}_{\mathrm{R}}\,|0_{\mathrm{R}}\rangle. \tag{B16}$$

This logic can be extended to arbitrary orders in $\dot{\phi}$. We can therefore obtain a good approximation by partially resumming, that is, summing only terms of the first type (without exponential suppression) for each order in $\dot{\phi}$. We find

$$\begin{aligned} g_{\mathrm{R}}(\dot{\phi}) &= g^{(1)}_{\mathrm{R}} + g^{(2)}_{\mathrm{R}} + g^{(3)}_{\mathrm{R}} + \ldots \\ &= \langle 0_{\mathrm{R}}|\Bigg[\bar{\mathcal{G}}_{\mathrm{R}} + \bar{\mathcal{G}}_{\mathrm{R}}\left(-\frac{\mathcal{Q}_{\mathrm{R}}}{\mathcal{H}_{\mathrm{R}} - \epsilon_0}\bar{\mathcal{G}}_{\mathrm{R}}\right) \\ &\quad + \bar{\mathcal{G}}_{\mathrm{R}}\left(-\frac{\mathcal{Q}_{\mathrm{R}}}{\mathcal{H}_{\mathrm{R}} - \epsilon_0}\bar{\mathcal{G}}_{\mathrm{R}}\right)\left(-\frac{\mathcal{Q}_{\mathrm{R}}}{\mathcal{H}_{\mathrm{R}} - \epsilon_0}\bar{\mathcal{G}}_{\mathrm{R}}\right) + \ldots\Bigg]|0_{\mathrm{R}}\rangle \\ &= \langle 0_{\mathrm{R}}|\left(\mathbb{1} + \bar{\mathcal{G}}_{\mathrm{R}}\frac{\mathcal{Q}_{\mathrm{R}}}{\mathcal{H}_{\mathrm{R}} - \epsilon_0}\right)^{-1}\bar{\mathcal{G}}_{\mathrm{R}}\,|0_{\mathrm{R}}\rangle. \end{aligned} \tag{B17}$$

Accordingly, the $\dot{\phi}$-dependent corrections to the overlap energy in the right chain take the form

$$i\frac{g_{\mathrm{R}}}{2}\gamma_4\gamma_3, \tag{B18}$$

with g_{R} as given in Eq. (8) in the main text.

Finally, we focus on terms that are proportional to the tunneling amplitude δ_t, starting with those that are zeroth order in $\dot{\phi}$, namely

$$\tfrac{1}{2}[\psi^{\dagger}_{\mathrm{L}}(\mathcal{P}_{\mathrm{L}}\mathcal{H}_{\mathrm{T}}(\phi)\mathcal{P}_{\mathrm{R}})\psi_{\mathrm{R}} + \psi^{\dagger}_{\mathrm{R}}(\mathcal{P}_{\mathrm{R}}\mathcal{H}^{\dagger}_{\mathrm{T}}(\phi)\mathcal{P}_{\mathrm{L}})\psi_{\mathrm{L}}]. \tag{B19}$$

The first term can be simplified to

$$\mathcal{P}_{\mathrm{L}}\mathcal{H}_{\mathrm{T}}\mathcal{P}_{\mathrm{R}} = \sum_{x,y=0,\tilde{0}} q^{(1)}_{xy}\,|x_{\mathrm{L}}\rangle\langle y_{\mathrm{R}}|, \tag{B20}$$

with

$$q^{(1)}_{xy}(\phi) = \langle x_{\rm L}|\,\mathcal{H}_{\rm T}(\phi)\,|y_{\rm R}\rangle\,. \tag{B21}$$

Substituting with $\mathcal{P}_{\rm L}\mathcal{H}_{\rm T}\mathcal{P}_{\rm R}$ into Eq. (B19) leads to

$$\begin{aligned}&\tfrac{1}{2}\big(q^{(1)}_{00}c^\dagger_{\rm L}c_{\rm R} + q^{(1)}_{\tilde{0}\tilde{0}}c_{\rm L}c_{\rm R} + q^{(1)}_{0\tilde{0}}c^\dagger_{\rm L}c^\dagger_{\rm R} + q^{(1)}_{\tilde{0}0}c_{\rm L}c^\dagger_{\rm R} + \text{H.c.}\big)\\ &\quad = q^{(1)}_{00}c^\dagger_{\rm L}c_{\rm R} - q^{(1)}_{\tilde{0}\tilde{0}}c^\dagger_{\rm R}c_{\rm L} + q^{(1)}_{\tilde{0}0}c_{\rm L}c_{\rm R} - q^{(1)}_{0\tilde{0}}c^\dagger_{\rm R}c^\dagger_{\rm L},\end{aligned} \tag{B22}$$

where $c_{\rm L}$ and $c_{\rm R}$ are defined in Eqs. (B10) and (B11), respectively. Alternatively, we can express the result in terms of the Majorana operators. In this case, Eq. (B22) takes the form

$$i\,\Re\left\{\frac{q^{(1)}_{00} - q^{(1)}_{0\tilde{0}}}{2}\right\}\gamma_2\gamma_3 = i\left(\frac{q^{(1)}_{00}(0) - q^{(1)}_{0\tilde{0}}(0)}{2}\right)\cos\left(\frac{\phi}{2}\right)\gamma_2\gamma_3, \tag{B23}$$

where, in leading order, the weak link only couples Majoranas γ_2 and γ_3.

As for the corrections of the electromotive force (emf) to tunneling across the junction, it suffices to only include corrections that are first order in $\dot{\phi}$, leading to

$$i\,\Re\left\{\frac{q^{(2)}_{00} - q^{(2)}_{0\tilde{0}}}{2}\right\}\gamma_2\gamma_3, \tag{B24}$$

where

$$\begin{aligned}q^{(2)}_{xy}(\phi) = -\frac{1}{2}\,\langle x_{\rm L}|\,\mathcal{H}_{\rm T}(\phi)\frac{\mathcal{Q}_{\rm R}}{\mathcal{H}_{\rm R} - \epsilon_x}\bar{\mathcal{G}}_{\rm R}\\ + \mathcal{H}_{\rm T}(\phi)\frac{\mathcal{Q}_{\rm R}}{\mathcal{H}_{\rm R} - \epsilon_y}\bar{\mathcal{G}}_{\rm R}\,|y_{\rm R}\rangle\,.\end{aligned} \tag{B25}$$

The tunneling terms therefore become

$$i\left(\frac{q_{00}(0) - q_{0\tilde{0}}(0)}{2}\right)\cos\left(\frac{\phi}{2}\right)\gamma_2\gamma_3, \tag{B26}$$

with

$$q_{xy}(\phi) = q^{(1)}_{xy}(\phi) + q^{(2)}_{xy}(\phi). \tag{B27}$$

In limit where only coupling between γ_2 and γ_3 across the weak link survives, we can simplify the coefficients to

$$q^{(1)}_{00}(0) \approx -q^{(1)}_{0\tilde{0}}(0) \approx \langle 0_{\rm R}|\,\mathcal{H}_{\rm T}(0)\,|0_{\rm R}\rangle\,, \tag{B28}$$

and

$$q^{(2)}_{00}(0) \approx -q^{(2)}_{0\tilde{0}}(0) \approx -\,\langle 0_{\rm L}|\,\mathcal{H}_{\rm T}(0)\frac{\mathcal{Q}_{\rm R}}{\mathcal{H}_{\rm R}}\bar{\mathcal{G}}_{\rm R}\,|0_{\rm R}\rangle\,. \tag{B29}$$

We can therefore rewrite Eq. (B26) as

$$iE_{\rm M}\,\cos\left(\frac{\phi}{2}\right)\gamma_2\gamma_3, \tag{B30}$$

with

$$E_{\rm M}(\dot{\phi}) = \langle 0_{\rm R}|\,\mathcal{H}_{\rm T}(0)\,|0_{\rm R}\rangle - \langle 0_{\rm L}|\,\mathcal{H}_{\rm T}(0)\frac{\mathcal{Q}_{\rm R}}{\mathcal{H}_{\rm R}}\bar{\mathcal{G}}_{\rm R}\,|0_{\rm R}\rangle\,. \tag{B31}$$

Adding Eqs. (B9), (B18), and (B31) leads to the low-energy Hamiltonian

$$H_{\rm low} = i\frac{\epsilon_0}{2}\gamma_2\gamma_1 + i\left(\frac{\epsilon_0 + g_{\rm R}}{2}\right)\gamma_4\gamma_3 + iE_{\rm M}\,\cos\left(\frac{\phi}{2}\right)\gamma_2\gamma_3. \tag{B32}$$

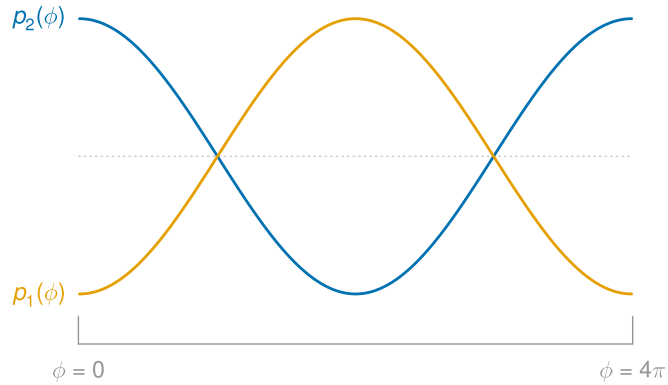

FIG. 7. Energy spectrum of Hamiltonian H_p in Eq. (9) in the main text with $\mathcal{E} = 0$. The zero gap occurs either due to the oscillatory behavior of $g_{\rm R}$ as a function of the voltage V (Fig. 2 in the main text), or simply when using the unrenormalized parameters that assumes the entire phase drop between the two superconductors can be included across the weak link.

Using Eq. (B10), we can decompose the low-energy Hamiltonian into two decoupled two-level systems for odd and even electron parities. The odd parity consists of the states $|01\rangle$ and $|10\rangle$, while the even parity of $|00\rangle$ and $|11\rangle$ [with $c^\dagger_{\rm L}c^\dagger_{\rm R}\,|00\rangle = |11\rangle$, and Eqs. (B10) and (B11) define $c_{\rm L}$ and $c_{\rm R}$, respectively]. The Hamiltonians of these two subspaces read

$$H_p = -\mathcal{E}\sigma_x + E_{\rm M}\cos\left(\frac{\phi}{2}\right)\sigma_z, \tag{B33}$$

where $\mathcal{E} \equiv \delta_{p,0}\,\epsilon_0 + g_{\rm R}/2$ with the integer $p = 0, 1$ for the even and odd parities, respectively.

APPENDIX C: STEADY-STATE DC CURRENT FOR THE UNGAPPED HAMILTONIAN

For a vanishingly small gap, the basis defined by the unitary transformation (11) in the main text is not suitable since the off-diagonal term (12) in the main text tends to a δ function. Instead, a suitable basis for the gapless system consists of the two uncoupled branches of $E_{\rm M}\cos(\phi/2)\,\sigma_z$ (Fig. 7). In this basis, we can obtain an analytical solution for the steady-state occupation probabilities and, subsequently, the dc current. For a gapless system, the two eigenstates are not coupled and the only process that changes the occupation probabilities is relaxation. Assuming a constant voltage V, it follows that $\phi(t) = 2eVt$ such that there is a one-to-one correspondence between time t, and ϕ at a given time. We therefore use the notation that when ϕ appears as an argument for the time evolution of the state, it should be interpreted as the time at which the phase assumes the value of ϕ (this avoids confusion with the tunneling parameter t in the Kitaev chain).

Starting from an initial value at $\phi = 0$ (Fig. 7), the probability at $\phi = \pi$ can be written as

$$\begin{aligned}p_1(\pi) &= p_1(0) + (1 - W)\,p_2(0)\\ &= p_1(0) + (1 - W)\,[1 - p_1(0)],\end{aligned} \tag{C1}$$

where $W \equiv \exp(-\pi\Gamma/\dot{\phi})$. Here, p_1 and p_2 represent the occupation probabilities of the two states of the Hamiltonian $E_{\rm M}\cos(\phi/2)\,\sigma_z$ as defined in Fig. 7 (i.e., at $\phi = 0$, p_1

corresponds to the ground state and p_2 to the excited state). Similarly, we can write the probability p_1 at $\phi = 3\pi$ as

$$p_1(3\pi) = W^2\, p_1(\pi), \tag{C2}$$

and, finally, at $\phi = 4\pi$ as

$$p_1(4\pi) = p_1(3\pi) + (1 - W)\,[1 - p_1(3\pi)]. \tag{C3}$$

In the steady state, we can impose the 4π-periodicity condition

$$p_1(4\pi) = p_1(0). \tag{C4}$$

Solving the four Eqs. (C1)–(C4) yields the steady-state probabilities

$$p_1(0) = 1 - \frac{W}{1 + W^2}, \tag{C5}$$

and

$$p_2(0) = \frac{W}{1 + W^2}. \tag{C6}$$

The values $\phi = 0$ can be readily used to obtain the probabilities as a function of ϕ. As for the current, its expected value is defined as $\mathrm{Tr}(\rho I)$, where the occupation probabilities are the diagonal elements of the density matrix ρ and with the current operator

$$I = eE_{\mathrm{M}}\, \sin\left(\frac{\phi}{2}\right)\sigma_z. \tag{C7}$$

The expected value of the current then reads

$$I^{\mathrm{gapless}} = e|E_{\mathrm{M}}|[1 - 2p_1(\phi)]\, \sin\left(\frac{\phi}{2}\right), \tag{C8}$$

with the superscript denoting that this expression is valid for the gapless system. Averaging over the period $[0, 4\pi]$ yields the steady-state dc current

$$\begin{aligned} I_{\mathrm{dc}}^{\mathrm{gapless}} &= \frac{e|E_{\mathrm{M}}|}{4\pi} \int_0^{4\pi} I^{\mathrm{gapless}}\, d\phi \\ &= -\frac{e|E_{\mathrm{M}}|}{\pi} \frac{4\Gamma\dot{\phi}}{4\Gamma^2 + \dot{\phi}^2}. \end{aligned} \tag{C9}$$

The analytical solution (C9) is valid at points where the new overlap energy g_{R} is zero (or vanishingly small) as a function of the voltage V [see Figs. 2 and 3(a) in the main text]. It is also used to obtain the dc current in Fig. 3(b) for the driven system without renormalizing the parameters [i.e., $g_{\mathrm{R}} = 0$ and $E_{\mathrm{M}} \to E_{\mathrm{M}}^0 = E_{\mathrm{M}}(\dot{\phi} = 0)$].

[1] A. Altland and M. R. Zirnbauer, Phys. Rev. B **55**, 1142 (1997).
[2] A. Kitaev, AIP Conf. Proc. **1134**, 22 (2009).
[3] S. Ryu, A. P. Schnyder, A. Furusaki, and A. W. W. Ludwig, New J. Phys. **12**, 065010 (2010).
[4] C. K. Chiu, J. C. Y. Teo, A. P. Schnyder, and S. Ryu, Rev. Mod. Phys. **88**, 035005 (2016).
[5] M. Leijnse and K. Flensberg, Semicond. Sci. Technol. **27**, 124003 (2012).
[6] P. Marra, J. Appl. Phys. **132**, 231101 (2022).
[7] J. Linder, T. Yokoyama, and A. Sudbø, Phys. Rev. B **80**, 205401 (2009).
[8] H.-Z. Lu, W.-Y. Shan, W. Yao, Q. Niu, and S.-Q. Shen, Phys. Rev. B **81**, 115407 (2010).
[9] C.-X. Liu, H. J. Zhang, B. Yan, X.-L. Qi, T. Frauenheim, X. Dai, Z. Fang, and S.-C. Zhang, Phys. Rev. B **81**, 041307(R) (2010).
[10] L. Fidkowski, R. M. Lutchyn, C. Nayak, and M. P. A. Fisher, Phys. Rev. B **84**, 195436 (2011).
[11] M. Cheng and R. Lutchyn, Phys. Rev. B **92**, 134516 (2015).
[12] M. McGinley and N. R. Cooper, Phys. Rev. Lett. **121**, 090401 (2018).
[13] M. McGinley and N. R. Cooper, Phys. Rev. B **99**, 075148 (2019).
[14] M. McGinley and N. R. Cooper, Nat. Phys. **16**, 1181 (2020).
[15] C.-E. Bardyn, L. Wawer, A. Altland, M. Fleischhauer, and S. Diehl, Phys. Rev. X **8**, 011035 (2018).
[16] K. Kawabata, K. Shiozaki, M. Ueda, and M. Sato, Phys. Rev. X **9**, 041015 (2019).
[17] R.-P. Riwar, Phys. Rev. B **100**, 245416 (2019).
[18] S. Lieu, R. Belyansky, J. T. Young, R. Lundgren, V. V. Albert, and A. V. Gorshkov, Phys. Rev. Lett. **125**, 240405 (2020).
[19] S. Lieu, M. McGinley, and N. R. Cooper, Phys. Rev. Lett. **124**, 040401 (2020).
[20] E. J. Bergholtz, J. C. Budich, and F. K. Kunst, Rev. Mod. Phys. **93**, 015005 (2021).
[21] A. Altland, M. Fleischhauer, and S. Diehl, Phys. Rev. X **11**, 021037 (2021).
[22] T.-S. Deng and L. Pan, Phys. Rev. B **104**, 094306 (2021).
[23] I. Mandal and E. J. Bergholtz, Phys. Rev. Lett. **127**, 186601 (2021).
[24] K. Kawabata, K. Shiozaki, and S. Ryu, Phys. Rev. B **105**, 165137 (2022).
[25] C.-H. Liu, H. Hu, and S. Chen, Phys. Rev. B **105**, 214305 (2022).
[26] A. M. García-García, L. Sá, and J. J. M. Verbaarschot, Phys. Rev. X **12**, 021040 (2022).
[27] M. A. Javed, J. Schwibbert, and R.-P. Riwar, Phys. Rev. B **107**, 035408 (2023).
[28] A. Messiah, *Quantum Mechanics* (North-Holland Publishing Company, Amsterdam, 1961), Vol. 1.
[29] X. You, J. A. Sauls, and J. Koch, Phys. Rev. B **99**, 174512 (2019).
[30] R.-P. Riwar and D. P. DiVincenzo, npj Quantum Inf. **8**, 36 (2022).
[31] J. Bryon, D. K. Weiss, X. You, S. Sussman, X. Croot, Z. Huang, J. Koch, and A. A. Houck, Phys. Rev. Appl. **19**, 034031 (2023).
[32] L. Fu and C. L. Kane, Phys. Rev. Lett. **100**, 096407 (2008).
[33] L. Fu and C. L. Kane, Phys. Rev. B **79**, 161408(R) (2009).
[34] S. Nadj-Perge, I. K. Drozdov, B. A. Bernevig, and A. Yazdani, Phys. Rev. B **88**, 020407(R) (2013).
[35] F. Pientka, L. I. Glazman, and F. von Oppen, Phys. Rev. B **88**, 155420 (2013).

[36] M. Hell, M. Leijnse, and K. Flensberg, Phys. Rev. Lett. **118**, 107701 (2017).
[37] F. Pientka, A. Keselman, E. Berg, A. Yacoby, A. Stern, and B. I. Halperin, Phys. Rev. X **7**, 021032 (2017).
[38] J. Alicea, Rep. Prog. Phys. **75**, 076501 (2012).
[39] M. Sato and Y. Ando, Rep. Prog. Phys. **80**, 076501 (2017).
[40] K. Flensberg, F. von Oppen, and A. Stern, Nat. Rev. Mater. **6**, 944 (2021).
[41] R. M. Lutchyn, J. D. Sau, and S. Das Sarma, Phys. Rev. Lett. **105**, 077001 (2010).
[42] Y. Oreg, G. Refael, and F. von Oppen, Phys. Rev. Lett. **105**, 177002 (2010).
[43] S. Kashiwaya and Y. Tanaka, Rep. Prog. Phys. **63**, 1641 (2000).
[44] F. Domínguez, O. Kashuba, E. Bocquillon, J. Wiedenmann, R. S. Deacon, T. M. Klapwijk, G. Platero, L. W. Molenkamp, B. Trauzettel, and E. M. Hankiewicz, Phys. Rev. B **95**, 195430 (2017).
[45] J. D. Sau and F. Setiawan, Phys. Rev. B **95**, 060501(R) (2017).
[46] J. J. Feng, Z. Huang, Z. Wang, and Q. Niu, Phys. Rev. B **98**, 134515 (2018).
[47] S. J. Choi, A. Calzona, and B. Trauzettel, Phys. Rev. B **102**, 140501(R) (2020).
[48] A. E. Svetogorov, D. Loss, and J. Klinovaja, Phys. Rev. Res. **2**, 033448 (2020).
[49] D. Frombach and P. Recher, Phys. Rev. B **101**, 115304 (2020).
[50] Z. Wang, J. J. Feng, Z. Huang, and Q. Niu, Phys. Rev. Lett. **129**, 257001 (2022).
[51] L. P. Rokhinson, X. Liu, and J. K. Furdyna, Nature Phys. **8**, 795 (2012).
[52] J. Wiedenmann, E. Bocquillon, R. S. Deacon, S. Hartinger, O. Herrmann, T. M. Klapwijk, L. Maier, C. Ames, C. Brüne, C. Gould, A. Oiwa, K. Ishibashi, S. Tarucha, H. Buhmann, and L. W. Molenkamp, Nature Commun. **7**, 10303 (2016).
[53] E. Bocquillon, R. S. Deacon, J. Wiedenmann, P. Leubner, T. M. Klapwijk, C. Brüne, K. Ishibashi, H. Buhmann, and L. W. Molenkamp, Nature Nanotechnol. **12**, 137 (2017).
[54] A.-Q. Wang, C.-Z. Li, C. Li, Z.-M. Liao, A. Brinkman, and D.-P. Yu, Phys. Rev. Lett. **121**, 237701 (2018).
[55] P. Schüffelgen, D. Rosenbach, C. Li, T. W. Schmitt, M. Schleenvoigt, A. R. Jalil, S. Schmitt, J. Kölzer, M. Wang, B. Bennemann, U. Parlak, L. Kibkalo, S. Trellenkamp, T. Grap, D. Meertens, M. Luysberg, G. Mussler, E. Berenschot, N. Tas, A. A. Golubov *et al.*, Nature Nanotechnol. **14**, 825 (2019).
[56] K. Le Calvez, L. Veyrat, F. Gay, P. Plaindoux, C. B. Winkelmann, H. Courtois, and B. Sacépé, Commun. Phys. **2**, 4 (2019).
[57] D. Rosenbach, T. W. Schmitt, P. Schüffelgen, M. P. Stehno, C. Li, M. Schleenvoigt, A. R. Jalil, G. Mussler, E. Neumann, S. Trellenkamp, A. A. Golubov, A. Brinkman, D. Grützmacher, and T. Schäpers, Sci. Adv. **7**, eabf1854 (2021).
[58] M. Bai, X.-K. Wei, J. Feng, M. Luysberg, A. Bliesener, G. Lippertz, A. Uday, A. A. Taskin, J. Mayer, and Y. Ando, Commun. Mater. **3**, 20 (2022).
[59] M. Rößler, D. Fan, F. Münning, H. F. Legg, A. Bliesener, G. Lippertz, A. Uday, R. Yazdanpanah, J. Feng, A. Taskin, and Y. Ando, Nano Lett. **23**, 2846 (2023).
[60] A. Kenawy, F. Hassler, and R.-P. Riwar, Phys. Rev. B **106**, 035430 (2022).
[61] A. Y. Kitaev, Phys.-Usp. **44**, 131 (2001).
[62] A. Vuik, D. Eeltink, A. R. Akhmerov, and M. Wimmer, New J. Phys. **18**, 033013 (2016).
[63] M. W. A. de Moor, J. D. S. Bommer, D. Xu, G. W. Winkler, A. E. Antipov, A. Bargerbos, G. Wang, N. van Loo, R. L. M. O. het Veld, S. Gazibegovic, D. Car, J. A. Logan, M. Pendharkar, J. S. Lee, E. P. A. M. Bakkers, C. J. Palmstrøm, R. M. Lutchyn, L. P. Kouwenhoven, and H. Zhang, New J. Phys. **20**, 103049 (2018).
[64] D. Rosenbach, K. Moors, A. R. Jalil, J. Kölzer, E. Zimmermann, J. Schubert, S. Karimzadah, G. Mussler, P. Schüffelgen, D. Grützmacher, H. Lüth, and T. Schäpers, SciPost Phys. Core **5**, 017 (2022).
[65] R. Winkler, *Spin-orbit Coupling Effects in Two-Dimensional Electron and Hole Systems* (Springer, Berlin, 2003).
[66] E. T. Mannila, V. F. Maisi, H. Q. Nguyen, C. M. Marcus, and J. P. Pekola, Phys. Rev. B **100**, 020502 (2019).